Electrochimica Acta 56 (2011) 1781–1785

Contents lists available at ScienceDirect

Electrochimica Acta

journal homepage: www.elsevier.com/locate/electacta

Localized corrosion behavior of scratches on nickel-base Alloy 690TT

Fanjiang Meng, En-Hou Han*,[1], Jianqiu Wang, Zhiming Zhang, Wei Ke

State Key Laboratory for Corrosion and Protection, Institute of Metal Research, Chinese Academy of Sciences, 62 Wencui Road, Shenyang 110016, PR China

ARTICLE INFO

Article history:
Received 30 June 2010
Received in revised form 9 August 2010
Accepted 9 August 2010
Available online 14 August 2010

Keywords:
Scratch
Localized corrosion
SECM
Crack initiation
Alloy 690

ABSTRACT

Localized corrosion of scratched Alloy 690TT was studied using scanning electrochemical microscopy (SECM) in 10 wt.% NaOH solution and atomic force microscopy (AFM) after short-time oxidation tests in high temperature high pressure water at 250 °C. The results show that the scratches detected by SECM displayed more extensive electrochemical activity. The scratch groove and the whole deformed region caused by scratching as anode corresponded to the peak of tip current. The oxides formed in 250 °C high purity pressurized water nucleated preferentially at the scratch groove and grew faster than non-scratched surface. The nano-grained scratch groove has more electrochemical reactivity than mechanical twins at scratch banks. The intense localized corrosion could contribute to crack initiation at the bottom of scratch groove.

1. Introduction

Alloy 600 has been used for steam generator (SG) tubing in pressurized water reactors (PWRs) since the late 1960s, but this alloy is prone to stress corrosion cracking (SCC) in pure water, both acidic and alkaline solutions, and in lead-containing solutions [1]. This persistent SCC of Alloy 600 led to the development of Alloy 690 as early as 1972. Alloy 690 is more resistant to SCC in pure water and in acidified solutions and has largely replaced Alloy 600 usually in the thermally treated form of Alloy 690TT. Corrosion of steam generator tubing is often associated with abnormal surface conditions such as surface dents or scratches, which are produced during manufacturing, transportation or assembly process. The Electric Power Research Institute (EPRI) reported in 2007 that SCC of Alloy 600 SG tubes in Oconee Unit 1 and Unit 2 have been associated with scratches which were introduced on the external surfaces of tube during insertion [2]. Similar SCC occurred at McGuire-1 and McGuire-2 in 1980s and 1990s [1,3]. These incidents indicate that mechanically produced marks and scratches can initiate SCC.

Meng et al. [4] have reported that preferential transgranular attack at the bank of scratches and intergranular stress corrosion cracking at the bottom of scratches in Alloy 690 in lead-containing caustic solution at 330 °C. What led to the preferential attack at the deformed scratches needs to be investigated. In general, small anodic areas correspond to severe corrosion problems with low detectability. Instead of conventional electrochemical techniques, scanning electrochemical microscopy (SECM), as a state-of-the-art local probing technique to image highly localized electrochemical currents near the surface, supplies a good technique to study the dynamic process of local sites. For example, SECM was employed to study the initiation and formation of localized corrosion pits on stainless steel and aluminum samples [5]. Preferential dissolution in the boundary region between some intermetallic particles and alloy matrix was observed by using atomic force microscopy (AFM) and SECM [6].

High-temperature oxidation of scratches is another aspect that should not be neglected. Sogo et al. [7] concluded that the high-temperature oxidation was regarded as a successive multi-nucleation process in a reaction–diffusion field after investigation of the initial oxidation of Ni (1 1 1) in the range of 550–700 K. Machet et al. [8] reported that the thin oxide film formed rapidly on Alloy 600 and revealed a terrace and step topography of the (1 1 1)-oriented surface of the Ni–19Cr–7Fe (at.%) single crystal after a passivation time of 1 min in 325 °C water. Effects of scratching on the re-oxidation of Fe-, Ni-, and Co-based alloy surfaces were studied and significant differences in the composition and hardness of re-oxidation products on the scratch groove were observed in 850 °C air [9]. The short-time oxidation is the nucleation and formation of oxides that are thermodynamically stable in given solution and the oxidation of local sites is sometimes decisive.

It is common sense that scratches introduced on alloys surface are harmful to the corrosion of materials. However, the effect of scratches on the dissolution and oxidation behavior of materials is not well understood and there is little work relating to localized corrosion on scratches. Based on the characterization of microstructure of scratches on the same nickel alloy in our previous work [4], SECM was used to characterize the local corrosion behavior at

* Corresponding author. Tel.: +86 24 23893841; fax: +86 24 23894149.
E-mail address: ehhan@imr.ac.cn (E.-H. Han).
[1] ISE member.

0013-4686/$ – see front matter © 2010 Elsevier Ltd. All rights reserved.
doi:10.1016/j.electacta.2010.08.028

scratches on Alloy 690 surface in order to reveal the stress corrosion mechanism at scratches.

2. Experimental

2.1. Material

The test material was Alloy 690TT, which was obtained from EPRI and had the following chemical composition Ni: 59.50, Cr: 29.02, S: 0.001, C: 0.018, Ti: 0.33, Mn: 0.30, P: 0.009, Si: 0.31, Cu: 0.01, Co: 0.015, Al: 0.16 in mass% and Fe: balance. The mill certification supplied with the bulk material identified a thermal treatment of 700 °C for 5 h.

2.2. Methods and techniques

The coupons of $10 \times 10 \times 3\,mm^3$ were cut from the bulk material and surfaces of the coupon were ground to 2000 grit with water proof paper and polished with 0.5 μm alumina to obtain a mirror finish. The polished surfaces were scratched with a well-controlled and monitored scratching device, which was depicted in previous work [4]. Two kinds of scratches were prepared on the polished surface of Alloy 690TT: 100 μm in width and 25 μm in depth for conducting scanning electrochemical microscopy measurements and 4 μm in width and 2 μm in depth for short-time oxidation tests. The scratches on Alloy 690TT were examined by using a FEI XL30 field emission environmental scanning electron microscopy (SEM) and surface profiler system Micro XAM-3D. The microstructure of the cross-section underneath the scratch was characterized using transmission electron microscopy (TEM). The TEM samples at the scratch were prepared using focus ion beam (FIB) FEI QUANTA 200 3D.

The coupons with big scratches were cut into pieces of $2 \times 2\,mm^2$ and the scratch was kept in the center of each piece. These pieces were welded with conducting wires and sealed in glass tubes with epoxy so that the scratched surface formed the testing substrate electrode. The test solution was aerated 10 wt.% NaOH solution (pH 13.8). The SECM information was obtained by scanning ultramicroelectrode (UME), which was Pt 10 μm in diameter, vertical to the scratches. Each specimen was immersed in the caustic solution for 30 min and a relatively stable open circuit potential (−0.55 vs. SCE/V) was recorded. Substrate generation and tip collection (SG/TC) mode was used, in which the substrate was held at the initial open circuit potential during the tests and the UME was biased at −0.45 vs. SCE/V to collect the ions generated by substrate. The UME was maintained at probe-substrate separation of about 15 μm.

Short-time oxidation of the fine scratch was performed at 250 °C in a 0.5 L autoclave which was specially designed for rapid cooling (~3 min) so that possible changes of the surface composition were minimized. Then the oxide film was analyzed ex situ at room temperature using PiscoScan 2500 AFM.

3. Results and discussion

3.1. Deformation caused by scratches

The surface morphology, both big scratches and small scratches were shown in Fig. 1. Fig. 1a shows the top view of the big scratch. The surface profile of the big scratch was shown in Fig. 1c. The scratch groove was very rough due to tearing. Both banks of the scratch were deformed heavily on the polished surface and the deformed region was about 50 μm at each bank of the scratch, which was similar to previous work [4]. The material from the scratch groove was ploughed out, pressed and piled at the bank

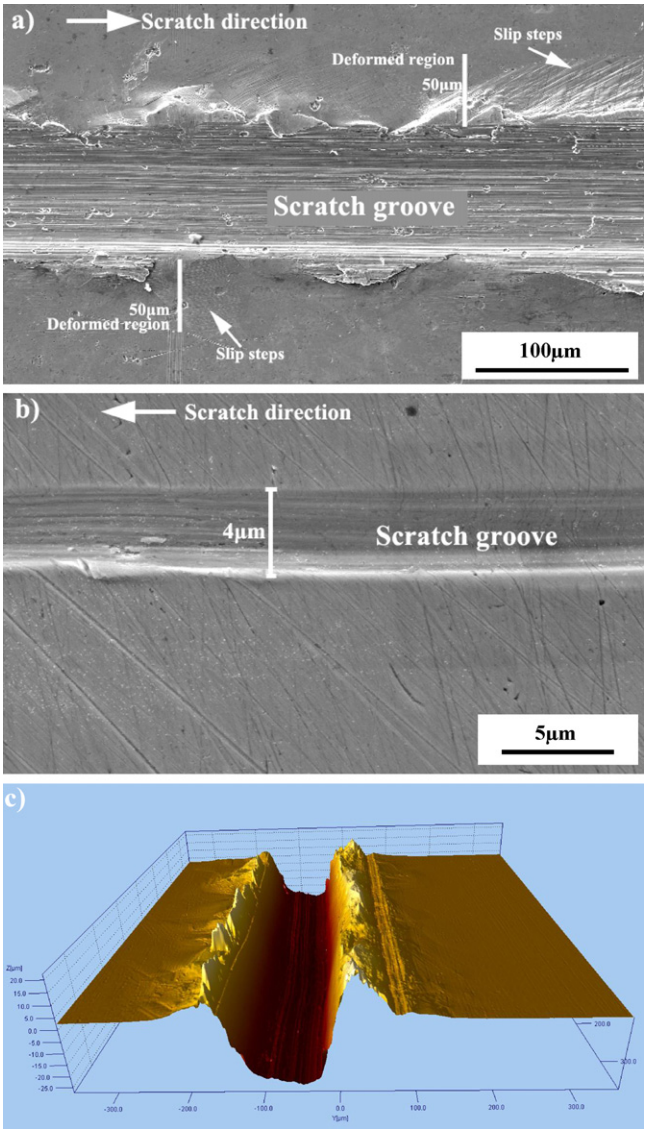

Fig. 1. Top view of aritificial scratches (a) the big scratch (100 μm in width, 25 μm in depth) for conducting SECM tests; (b) the slight scratch (4 μm in width, 2 μm in depth) for oxidation test; (c) surface profile of the big scratch.

of the scratch. There were two bumps beside the scratch groove as shown in Fig. 1c. The slight scratch is shown in Fig. 1b. The scratch groove was also rough, but the deformation at both banks caused by scratching was not obvious.

The etched cross-section of the scratch with several micro-sized grains was observed using SEM as is shown in Fig. 2a. There was a deformed layer about 20 μm in depth at the bottom of the scratch and the grain boundary was heavily deformed and curved. The TEM sample was sectioned using FIB at the scratch bottom and scratch bank. At the bottom of the scratch, instead of micro-sized grains, nano-grains were observed by TEM as shown in Fig. 2b. At the bank of the scratch, the mechanical twins were formed due to scratching as shown in Fig. 2c. For the Ni-based alloy, Alloy 600 with a low stack fault energy (SFE), when the sample was treated by surface mechanical attrition treatment (SMAT) [10], the cross-sectional TEM observations of the sample showed gradient structures in the surface layer, including randomly-oriented equiaxed nanocrystallites, mechanical nano-sized twins and planar dislocation arrays with the increasing depth. For the scratched surface, besides the gradient structure at the depth direction, there are gradient structures from the central line of the scratch to the free surface along

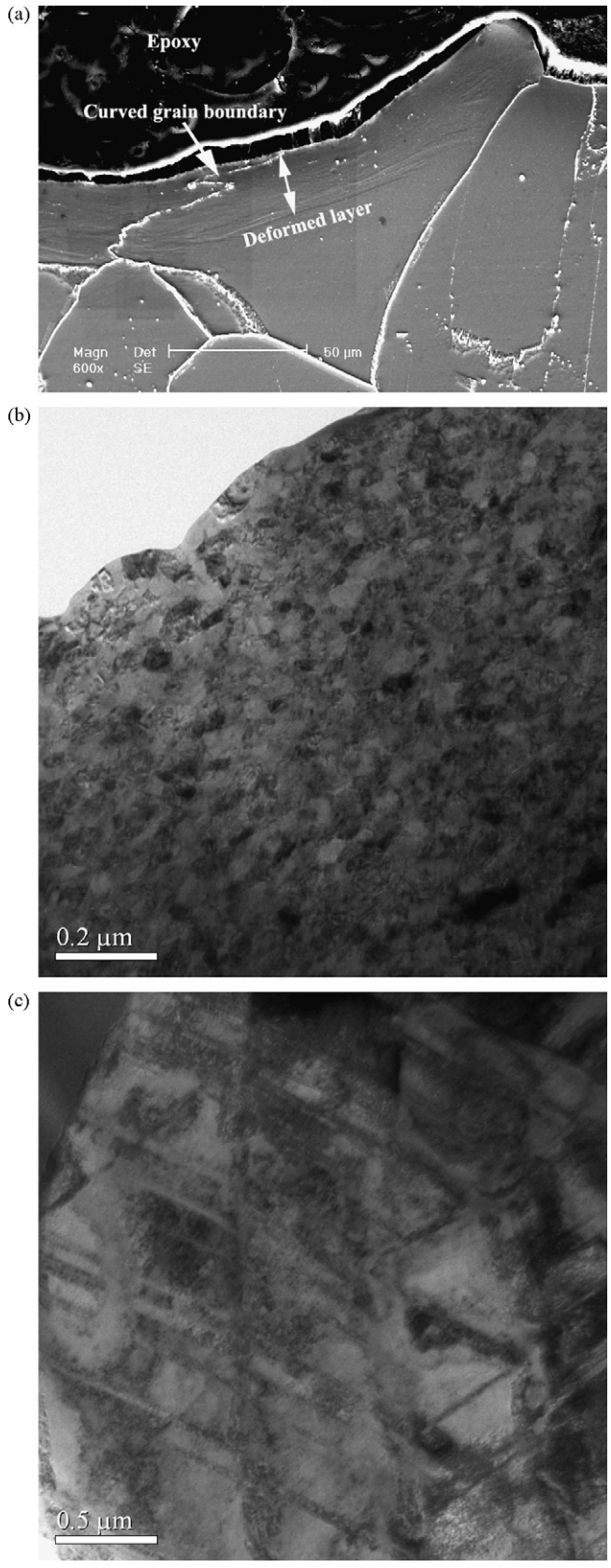

Fig. 2. Cross-section of the scratch (a) SEM observation, (b) TEM observation of the nano-grains at the bottom of the scratch, (c) TEM observation of the mechanical twins at the bank of the scratch.

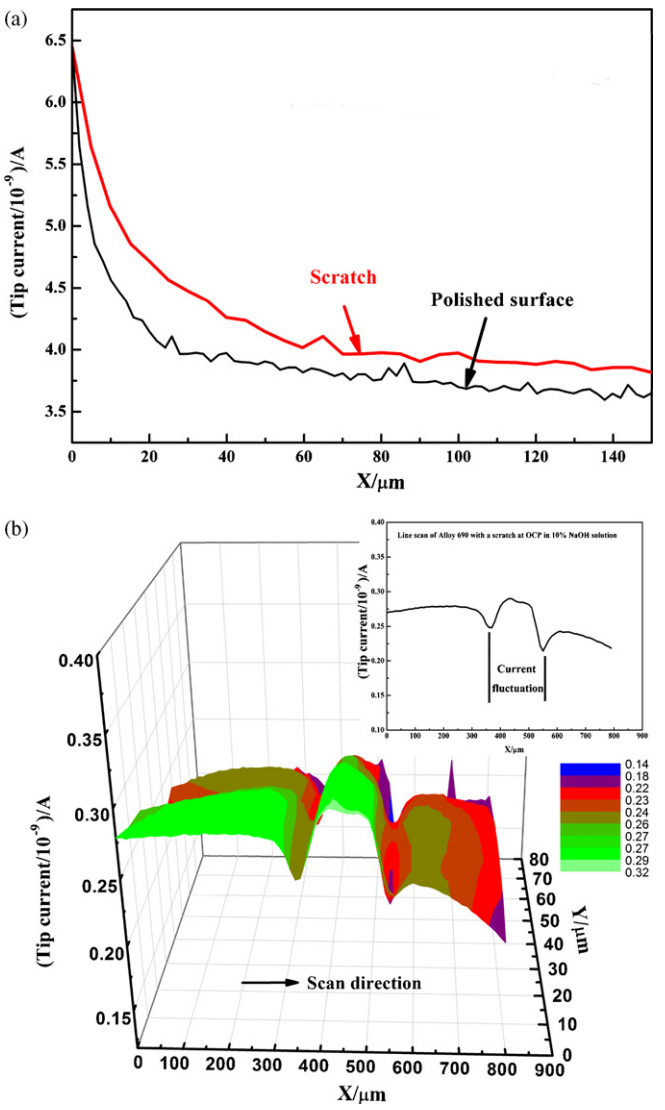

Fig. 3. (a) Approach curves of Alloy 690TT with a scratch at OCP in wt.10% NaOH solution; (b) SECM topography imaging of Alloy 690TT with a scratch at OCP in 10 wt.% NaOH solution. Tip potential: −0.45 vs. SCE/V, tip diameter: 10 μm, tip-substrate distance: 15 μm.

the surface direction. The nanostructured grains formed at the bottom of the groove, and at the banks of the scratches, the prominent feature of microstructure is mechanical twins. These mechanical twins are parallel to each other, and the intersection of mechanical twins in two directions is usually observed.

3.2. Electrochemical corrosion behavior at surface scratch

The local corrosion of scratches in Alloy 690 was studied using SECM in aerated 10 wt.% NaOH solution (pH 13.8). An SECM approach curve was obtained when the UME moved away from surface in the vertical direction to the surface. In order to keep the UME tip above the center of the scratch groove every time, the tip was lowered in vertical direction and moved horizontally until it slightly touched one of the bumps as described in Fig. 1c according to the CCD camera video. Then the UME tip continued to be moved horizontally with a distance of 50 μm which was the half width of the scratch. Finally, the tip was adjusted to the same height before it was lowered and approach curve was measured. As shown in Fig. 3a, the two approach curves achieved while UME was above polished surface and the scratch respectively, exhibited a sharp cur-

rent decrease as the UME went away from the surface at steps of 2 μm.

However, while the UME tip above the polished surface and scratch was at the same height, the tip current above the scratch was bigger than that above the polished surface. When the UME continued to move up to some distance, it could not collect the signal from local region, only an overall signal from the background. Fig. 3a also indicates that the collected signal above the scratch was sensed at a longer distance. The local current from polished surface could be collected for distances less than 30 μm, but above the scratch the local current was collected even for a tip distance of 60 μm, which means that the local electrochemical reaction at the scratch was more intense.

An area of $900 \times 80\ \mu m^2$ with a scratch in the middle was scanned as shown in Fig. 3b. The current map on the scratched surface indicates that there was a current peak above the scratch groove. There were two little current troughs beside the scratch which was smaller than the current on the polished surface as shown in the inset of Fig. 3b. The current at the UME was related to the distance between UME tip and surface [11]. During scanning the UME tip was kept at a constant height above the polished surface. This means the distance between the UME tip and the lowest point of the scratch groove was larger than other positions, so the current at the scratch groove should be much higher than the measured current value. Völker et al. [12] have also found a remarkable increase of tip current over a scratch in low carbon steel surfaces coated with tin because of dissolution of Fe. The increase of current at the UME indicates that corrosion rate over the scratch was faster compared to the polished surface in this caustic solution. Moreover, the tip current above the groove is bigger than that above the two piles beside the groove. It also indicates that the dissolution at the groove with nano-grain structure is more intense than that at the slip bands with mechanical twins. The distance between the two tip current troughs was 200 μm as depicted in the inset in Fig. 3b. It should be noticed the total deformed width caused by the scratch was about 200 μm (Fig. 1a), which indicates that the fluctuation of tip current was strongly related to the deformation.

Scratching created a deformed rough surface (Fig. 1a) including the scratch groove and scratch banks. Based on terrace–ledge–kink (TLK) model of a surface [13], as indicated by the increasing local dissolution current (Fig. 3a and b), the increased activity is associated with the irregular arrangement of Ni, Cr, Fe atoms in crystalline lattice. Atoms associated with a slip plane in presence of short-range order were more readily dissolved into the solution [14,15]. Thus, it is easy to understand the current increase above the scratch banks showed in Fig. 1a. Meng et al. found the tunnel corrosion at the slip bands on the scratch banks in acidic sodium solution and the stress corrosion cracking along the slip bands [4]. Although the distance between the UME tip and the two bumps beside the scratch groove was the shortest, the current above the bumps was not bigger than the current above the scratch groove. It indicates that the grain refinement by nanocrystallization at the scratch groove stores more deformation energy and has more electrochemical reactivity than the mechanical twins at the scratch banks.

According to Gutman [16], deformation changes surface micro-electrochemical heterogeneity and increases the local standard potential. Thus, the deformed region can act as the anode. The electrochemical activity in the slip steps is higher than non-slipped surface. The deformation causes a different energy distribution around the scratch. The local material at the scratch stored more deformation energy than polished surface away from the scratch. As schematically shown in Fig. 4, the whole current fluctuation region corresponding to the scratch groove and deformed region at both sides acted as the anode and this region was polarized to a more negative potential. For the counterpart of the anode, the polished surface beside the scratch deformed region as displayed in Fig. 1a acted cathodically (Fig. 3). Therefore, as the anode, the metal at the deformed region dissolved into solution as metal

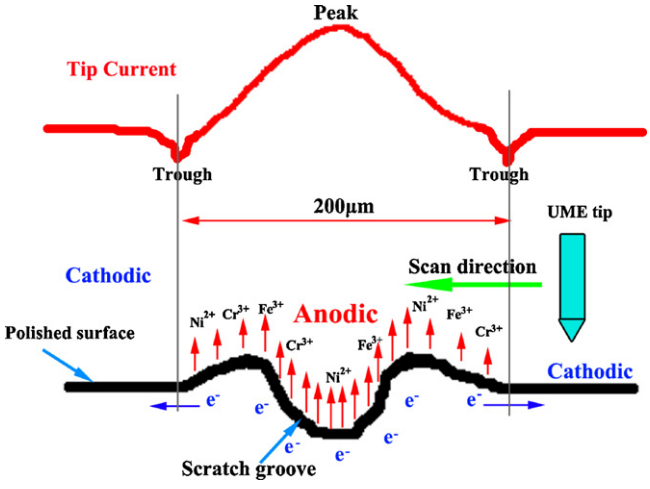

Fig. 4. Schematic representation of collected current at UME tip over one scratch for Alloy 690TT.

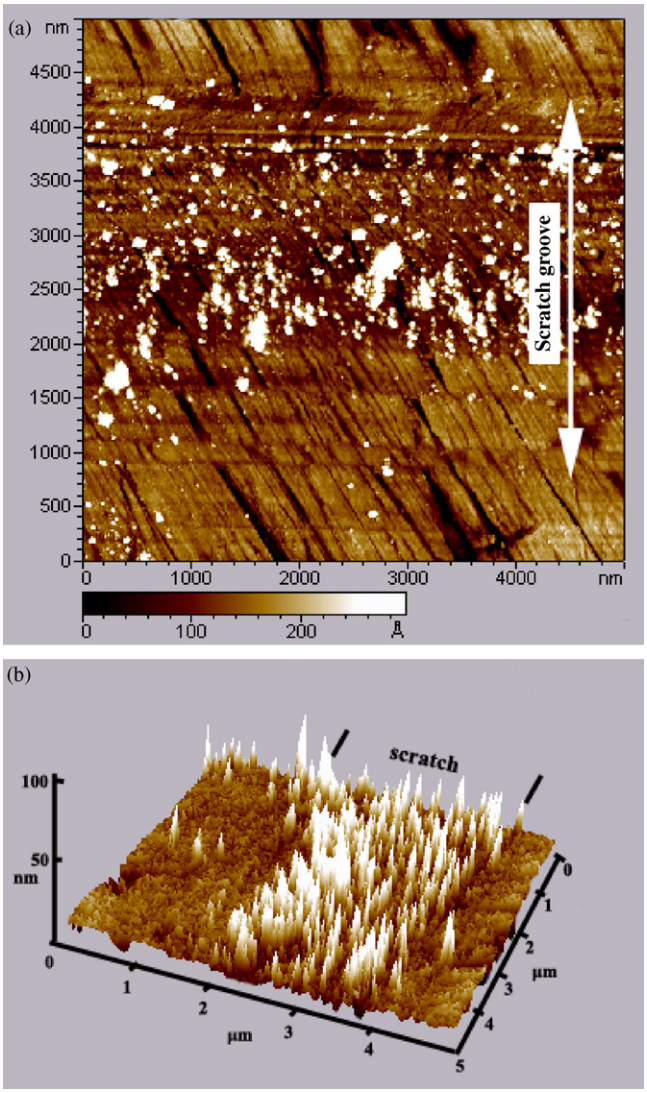

Fig. 5. AFM images for scratched Alloy 690TT after conducting oxidation test in 250 °C water for 2 min. (a) 2D oxides morphology; (b) 3D oxides morphology.

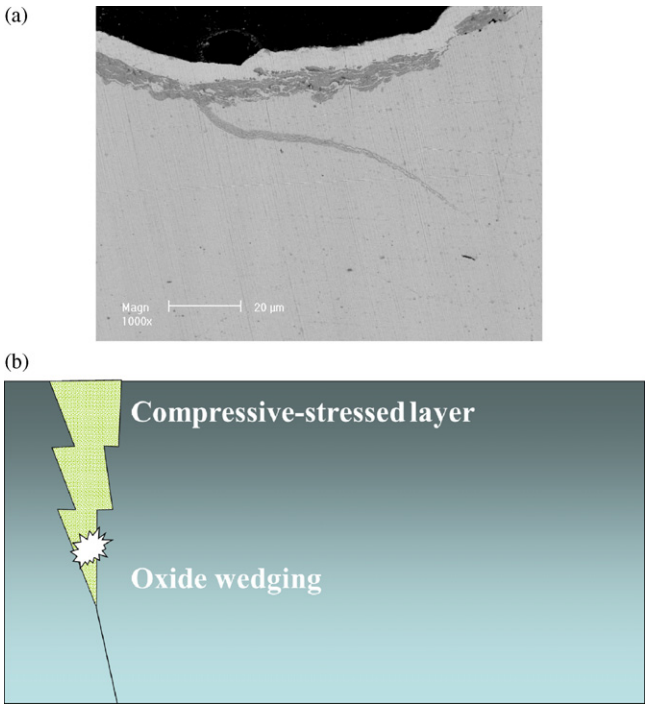

Fig. 6. (a) Crack initiation at the bottom of scratch groove in lead-containing caustic solution at 330 °C for 30 days [4]; (b) schematic drawing of SCC initiation mechanism at macro-compressive-stressed layer.

ions, and the left free electrons migrated towards to the cathode, the polished surface. At the edge between the anode and cathode, the free electrons density could be the highest and formed the current troughs as shown in Fig. 4. This agrees with a localized corrosion phenomenon which has been theoretically studied and experimentally observed by SVET measurements [17]. The UME tip current gained over scratch also reflects the dissolved microchemical species changes at the substrate/solution interface. However, the reactions occurred at the UME tip are not confirmed yet.

Short-time oxidation behavior of scratches in high temperature water was studied using AFM. Fig. 5a shows a 2D AFM image of short-time oxidation of Alloy 690TT with a slight scratch after 2 min of exposure in 250 °C water. Oxides did not homogeneously cover the Alloy 690TT surface with the fine scratch. Oxides preferentially grew at the scratch groove and oxides on the non-scratched surface are not obvious after short-time exposure. Fig. 5b gives a more clear 3D oxide morphology, which indicates that oxide on the scratch groove grew earlier and faster than the non-scratched surface. This is further evidence that corrosion at the scratch sites preferentially occurred in high temperature water.

The intergranular stress corrosion crack initiation as shown in Fig. 6a has been observed in our previous study [4]. An EPRI report [1] has mentioned that scratching can cause compressive stress at the scratched surface. The curved grain boundary and the deformation bands at the bottom of the scratch in Fig. 2a also show the compressive deformation. Inside the intergranular crack, the oxide is obvious. The crack initiation at the macro-compressive stressed area could be caused by the local tensile stress due to oxide wedging at the tip of the oxidized grain boundary. This process is schematically illustrated in Fig. 6b.

Utilizing SECM and AFM to study Alloy 690 with scratches, has resulted in a more detailed understanding of the localized corrosion processes on scratches at a microscopic level. The most intense electrochemical corrosion at the nano-grained scratch groove was induced by the whole deformed layer. The localized corrosion at the crack tip shown in Fig. 6a [4] could be the important contributor for the current peak above the scratch groove. Although scratching caused compressive stress underneath the scratch [1], the localized corrosion at the tip of the flaw forms oxide which wedges the flaw front to initiate SCC even at the macro-compressive layer as schematically shown in Fig. 6b.

4. Conclusions

Dissolution and short-time oxidation behavior at the scratch were investigated using SECM and AFM, respectively. The following conclusions can be derived from the results obtained:

The deformed scratch groove and scratch banks store more deformation energy, and anodically dissolve to form the current peak in 10% NaOH solution. The oxides nucleated preferentially at the scratch groove in 250 °C high temperature high pressure water and grew faster than non-scratched surface. The nano-grained scratch groove has more electrochemical reactivity than mechanical twins at scratch banks. The intense localized corrosion would contribute to crack initiation at the bottom of scratch groove.

Acknowledgements

This work is supported by the Special Funds for the Major State Basic Research Projects G2006CB605000. The authors gratefully acknowledge EPRI for providing commercial bulk Alloy 690TT. We also thank the assistance of Professor Shenhao Chen and Professor Lin Niu from Shandong University for performing SECM tests.

References

[1] R.W. Staehle, J.A. Gorman, Corrosion 59 (2003) 931.
[2] EPRI Report TR-106863, Oconee 2 Steam Generator Tube Examination.
[3] P.E. MacDonald, V.N. Shah, L.W. Ward, P.G. Ellison, Steam generator tube failures[R]. NUREG/CR-6365.
[4] F. Meng, J.Q. Wang, E.-H. Han, W. Ke, Corrosion Science 51 (2009) 2761.
[5] D.O. Wipf, Colloids and Surfaces A: Physicochemical and Engineering Aspects 93 (1994) 251.
[6] A. Davoodi, J. Pana, C. Leygraf, S. Norgren, Applied Surface Science 252 (2006) 5499.
[7] M. Sogo, T. Kamada, M. Aoki, S. Masuda, Surface Science 601 (2007) 3988.
[8] A. Machet, A. Galtayries, S. Zanna, L. Klein, V. Maurice, P. Jolivet, M. Foucault, P. Combrade, P. Scott, P. Marcus, Electrochimica Acta 49 (2004) 3957.
[9] P. Blau, T. Brummett, B. Pint, Wear 267 (2009) 380.
[10] N.R. Tao, J. Lu, K. Lu, Materials Science Forum 579 (2008) 91.
[11] Y. González-García, J.J. Santanal, J. González-Guzmán, J. Izquierdo, S. González, R.M. Souto, Progress in Organic Coatings. doi:10.1016/j.porgcoat.2010.04.006.
[12] E. Völker, C. Inchauspe, E. Calvo, Electrochemistry Communications 8 (2006) 179.
[13] B. Craig, Fundamental Aspects of Corrosion Films in Corrosion Science, Plenum Press, New York, 1991.
[14] H. Pickering, P. Swann, Corrosion 19 (1963) 373t.
[15] D. Tromans, J. Nutting, Corrosion 21 (1965) 143.
[16] E. Gutman, Mechanochemistry of Solid Surfaces, World Scientific Publishing Co. Pte. Ltd., Singapore, 1994.
[17] S. Rossi, M. Fedel, F. Deflorian, M. del Carmen Vadillo, Comptes Rendus Chimie 11 (2008) 984.